Effects of strong electronic interactions on the thermopower properties of the repulsive Hubbard model

Willdauany C. de Freitas Silva, Maykon V. Araujo, Sayantan Roy, Abhisek Samanta, Natanael de C. Costa, Nandini Trivedi, and Thereza Paiva

The effects of strong electronic interactions on the thermopower properties

Willdauany C. de Freitas Silva,[1] Maykon V. Araujo,[2] Sayantan Roy,[3] Abhisek Samanta,[3] Natanael de C. Costa,[1] Nandini Trivedi,[3] and Thereza Paiva[1]

[1]*Instituto de Física, Universidade Federal do Rio de Janeiro, Rio de Janeiro, RJ 21941-972, Brazil*
[2]*Departamento de Física, Universidade Federal do Piauí, 64049-550 Teresina PI, Brazil*
[3]*Department of Physics, The Ohio State University, Columbus OH 43210, USA*
(Dated: June 30, 2023)

We obtain the Seebeck coefficient or thermopower S, which determines the conversion efficiency from thermal to electrical energy, for the two-dimensional Hubbard model on different geometries (square, triangular, and honeycomb lattices) for different electronic densities and interaction strengths. Using Determinantal Quantum Monte Carlo (DQMC) we find the following key results: (a) the bi-partiteness of the lattice affects the doping dependence of S; (b) strong electronic correlations can greatly enhance S and produce non-trivial sign changes as a function of doping especially in the vicinity of the Mott insulating phase; (c) $S(T)$ near half filling can show non-monotonic behavior as a function of temperature. That is, our results show that electronic interactions lead to unexpected behavior for the thermopower for given fillings, even at high temperatures, which may vary depending on the geometry. We emphasize the role of strong interaction effects in engineering better devices for energy storage and applications, as captured by our calculations of the power factor $PF = S^2\sigma$ where σ is the dc conductivity.

I. INTRODUCTION

Over the past decades, a great deal of interest has been given to increasing the efficiency of electrical devices. As a possible route to this end, the thermoelectric materials may play a crucial role, once they exhibit induced voltage in presence of a temperature gradient. The efficiency of these materials is measured through parameters that composed the Figure of Merit, such as the Seebeck coefficient (thermopower) and the thermoelectric Power Factor [1]. However, there are many technical issues that make the development of efficient thermoelectric materials a challenge, e.g., the toxicity of the compounds, or their thermal instability. There are few ways to overcome these problems: (i) optimizing the already known compounds through band-structure engineering and nanostructuration techniques [2–4], or (ii) seeking new classes of compounds which exhibit unconventional properties usually related to strong electron-electron interactions [5]. In view of the increasing number of novel correlated compounds, controlling and manipulating geometry and correlations to enhance the thermopower properties is an open issue.

Despite intense experimental efforts, further theoretical investigations are required, in particular to understand interacting electronic compounds, such as Na_xCoO_2 or $FeSb_2$, which exhibit unusual large thermopower response [5–7]. In the former, the combination of quasi two-dimensional character with band topology and strong electronic correlations make this material an interesting playground to examine thermoelectricity. Once the charge carriers are confined to the hexagonal layers of Co atoms, a disordered distribution of Na ions above and below it can induce a charge imbalance. Using local-density approximation

and dynamical mean-field theory, Held et al [5] showed that disorder combined with the pudding-mold band structure and strong correlations enforce the electron-hole imbalance and enhances the thermopower by 200% with respect to the non-interacting case.

The thermopower of superconducting cuprates has been experimentally studied [8–11], with different compounds displaying very similar behavior with a sign change of the Seebeck coefficient near the maximum critical temperature [8]. This nearly universal behavior has been the subject of theoretical interest, being ascribed to a possible underlying critical point [12], to the presence of a van Hove singularity [13], and has been recently observed for the Hubbard Model with next-nearest neighbor hopping [14].

In view of these stimulating results, we explore how electron-electron interactions and geometry affect the Seebeck coefficient, and the thermoelectric Power Factor. In order to avoid the complexities behind the geometries and atomic orbitals present in real compounds, here we examine single band cases, to further understand the main effect of the correlations (from exact methodologies) on the thermopower properties. That is, our findings may shed light on so far unclear anomalous behavior of the Seebeck coefficient, in particular its sign change [15, 16]. To this end, we use unbiased Quantum Monte Carlo simulations to study the single band repulsive Hubbard model. We analyze the thermoelectric and electrical transport properties in the long wavelength DC limit in two-dimensions, in the square, triangular and honeycomb lattices. Our study finds a strong influence of particle hole symmetry of the many body spectrum and DOS on the behavior of the Seebeck coefficient with respect to doping. We show non trivial sign changes of the Seebeck coefficient that signal a deviation of the

Fermi surface from the Luttinger count and a subsequent anomalous change of the type of carriers below and above half filling. The sign change is also accompanied by a significant increase of the Seebeck coefficient near half filling with respect to the non-interacting and weakly interacting case. We show that despite using a simplified thermodynamic formula for the Seebeck coefficient that is independent of dynamical quantities, we are able to capture the effects of strong correlation.

The paper is organized as follows: In Section II we discuss the Hubbard model, an introduction to the Seebeck coefficient, Kelvin formula and the auxiliary field QMC method used to solve it. In Section III we discuss how to calculate the entropy and present our results for this quantity. Section IV shows the Local Density of States and conductivity results. In Section V we discuss the Seebeck coefficient and in Section VI the Power Factor. Finally, in section VIII we summarize our findings.

II. MODEL AND METHODS

The repulsive Fermi Hubbard model describes electrons on a lattice with an onsite repulsive interaction, with the Hamiltonian

$$
\mathcal{H} = -t \sum_{\langle \mathbf{i}, \mathbf{j} \rangle, \sigma} \left(c^\dagger_{\mathbf{i}, \sigma} c_{\mathbf{j}, \sigma} + \text{H.c.} \right) - \mu \sum_{\mathbf{i}, \sigma} n_{\mathbf{i}, \sigma}
$$
$$
+ U \sum_{\mathbf{i}} (n_{\mathbf{i}, \uparrow} - 1/2)(n_{\mathbf{i}, \downarrow} - 1/2), \qquad (1)
$$

where the sums run over sites of a given two-dimensional lattice, with $\langle \mathbf{i}, \mathbf{j} \rangle$ denoting nearest-neighbor sites. Here, we use the second quantization formalism, with $c^\dagger_{\mathbf{i}, \sigma}$ $(c_{\mathbf{i}, \sigma})$ being creation (annihilation) operators of electrons on a given site $\mathbf{i}$, and spin σ, while $n_{\mathbf{i}, \sigma} \equiv c^\dagger_{\mathbf{i}, \sigma} c_{\mathbf{i}, \sigma}$ are number operators. The first two terms on the right-hand side of Eq. (1) correspond to the hopping of electrons, and the chemical potential μ, respectively, with the latter determining the filling of the lattice. The third term describes the local repulsive interaction between electrons, with interaction strength U; the factor of $1/2$ is introduced to ensure invariance of the hamiltonian under particle-hole transformations on bipartite lattices. This implies that for the bipartite lattices we consider here (square and honeycomb lattices), $\mu = 0$ sets half-filling for all temperatures, and interaction strengths.

Our central quantities of interest are the transport coefficients, and their behavior with respect to doping and strength of interactions. The transport coefficients are defined through the following relations,

$$
\vec{j} = \overleftrightarrow{L}^{11} \vec{E} + \overleftrightarrow{L}^{12}(-\vec{\nabla}T)
$$
$$
\vec{j}^q = \overleftrightarrow{L}^{21} \vec{E} + \overleftrightarrow{L}^{22}(-\vec{\nabla}T) \qquad (2)
$$

where $\vec{j}$ and $\vec{j}^q$ are the electrical and thermal currents, and the $\overleftrightarrow{L}$s are rank 2 tensors defining conductivities

of the system. The tensors $\overleftrightarrow{L}^{11}$ and $\overleftrightarrow{L}^{22}$ are the electrical and thermal conductivities, and $\overleftrightarrow{L}^{12}(\overleftrightarrow{L}^{21})$ are the thermoelectrical(electrothermal) conductivities. The thermopower or Seebeck coefficient is defined as

$$
S = \frac{(\overleftrightarrow{L}^{12})_{xx}}{(\overleftrightarrow{L}^{11})_{xx}} = \frac{1}{T} \frac{(\overleftrightarrow{L}^{21})_{xx}}{(\overleftrightarrow{L}^{11})_{xx}}, \qquad (3)
$$

where the second equality is due to Onsager's reciprocity relations[17]. Using linear response theory with respect to electrical field and temperature, the Seebeck coefficient in the Kubo formalism can also be written as

$$
S(q_x, \omega) = \frac{1}{T} \frac{\chi_{\hat{\rho}(q_x), \mathcal{H}(-q_x)}(\omega)}{\chi_{\hat{\rho}(q_x) \hat{\rho}(-q_x)}(\omega)} \qquad (4)
$$

where

$$
\chi_{\hat{\rho}(q) \mathcal{H}(-q)}(\omega) = \lim_{\eta \to 0} \sum_{n,m} (f_n - f_m) \frac{\langle n | \hat{\rho}(q) | m \rangle \langle m | \mathcal{H}(-q) | n \rangle}{\omega + i\eta + \epsilon_n - \epsilon_m}
$$
$$
\chi_{\hat{\rho}(q) \hat{\rho}(-q)}(\omega) = \lim_{\eta \to 0} \sum_{n,m} (f_n - f_m) \frac{\langle n | \hat{\rho}(q) | m \rangle \langle m | \hat{\rho}(-q) | n \rangle}{\omega + i\eta + \epsilon_n - \epsilon_m}
$$
$$
(5)
$$

define the electrothermal and electrical conductivities, respectively. The operator $\hat{\rho}(q)$ is the charge density at a wave vector q, defined by

$$
\hat{\rho}(q) = \sum_{k, \sigma} \hat{c}^\dagger_{k+q, \sigma} \hat{c}_{k, \sigma} \qquad (6)
$$

and $\mathcal{H}(q)$ is the Fourier transform of the Hamiltonian. Evaluation of a Kubo-like formula (Eq (4)) is not easy for interacting systems in the thermodynamic limit, although it is the most insightful. Alternate formulas like the Mott formula[18], Heikes-Mott[19], high frequency Seebeck[20–22] and Kelvin formula[21, 23] exist but are limited by their applicability to specific scenarios (weakly correlated metal at low temperatures for the Mott formula, high-temperature limit for the Heikes-Mott formula, and measurement of transport at high frequencies compared to characteristic energy scale for high-frequency Seebeck formula). The Kelvin formula was proposed by Lord Kelvin to provide reciprocity between Seebeck and Peltier coefficients, and is calculated in the slow limit $(q_x \to 0, \omega \to 0)$; it can be derived by taking the slow limit of Eq (4) [23]. The Kelvin formula for the Seebeck coefficient is

$$
S_{\text{Kelvin}} = -\frac{1}{e} \frac{\partial \mu}{\partial T} \bigg|_{V,n} = \frac{1}{e} \frac{\partial s}{\partial n} \bigg|_{T,V},
$$

where the second equality follows from Maxwell's relations. Although expressed in terms of thermodynamic quantities, which are sufficient to capture the effects from the many-body density of states, it misses kinematic factors like contributions

from velocities at the Fermi surface and relaxation times. Nonetheless, the effects of strong correlations on the low-frequency transport behavior are taken into account, as it retains the $\omega < U$ approximation, which the high frequency formula, S^* misses. The justification and benchmark of using the Kelvin formula for strongly interacting systems like the Hubbard model and fractionalized systems like $\nu = 5/2$ FQHE states have already been established[23, 24].

We investigate the thermodynamics and transport properties of Eq. (1) on three different lattices: square, triangular and honeycomb. In particular, we examine the behavior of the entropy, conductivity, Local Density of States (LDOS), Seebeck coefficient, and Power Factor as functions of lattice filling, for different values of interaction strengths. To this end, we perform unbiased determinant quantum Monte Carlo (DQMC) simulations [25–28], a state-of-the-art numerical method that maps a many-particle interacting fermionic system into a single-particle (quadratic form) one, with the aid of bosonic auxiliary fields. More details about the methodology may be found in, e.g., Refs. 29–31, and references therein. Our DQMC simulations are performed for finite-sized systems (with 100, 144 and 162 sites for the square, triangular, and honeycomb lattices, respectively), with a Trotter step size $\Delta\tau \leq 0.1$ and each run is generated with 2000 warmup passes and 50000 measurement passes. Throughout this work, unless otherwise indicated, we consider for interaction strengths $U/t = 0$, 2, 4, 6, 8, and 10; i.e., from non-interacting to strong coupling regimes and $T/t = 0.5$, which corresponds to an energy scale low enough to observe the crossover towards an insulating phase at half-filling [32–34]. Hereafter, we define the lattice constant as unity, and the hopping integral t as the energy scale. Finally, our simulations have the infamous minus-sign problem of the fermion determinant, which requires longer runs, and constrains the scales of our temperatures and interaction strengths.

III. ENTROPY

We start our analysis with the electronic density n as a function of chemical potential μ shown in Figure 1 for $T/t = 0.5$ and the different lattices studied: (a) square, (b) triangular, and (c) honeycomb. To obtain this Figure, we gathering density data on a fine grid of chemical potentials. Particle-hole symmetry is evident for the square and honeycomb lattices, where $n(\mu) = 2 - n(-\mu)$, thereby the density data only need to be gathered either above or below half-filling. We employ a grid of $\Delta\mu = 0.20$ or 0.25 for fillings $0.1 \lesssim n \lesssim 0.9$, and $\Delta\mu = 0.5$ out of this range. In all geometries, correlations lead to the formation of a Mott plateau (insulating phase) around half-filling, although the critical interaction strength for the onset of "Mottness" is strongly influenced by the lattice geometry.
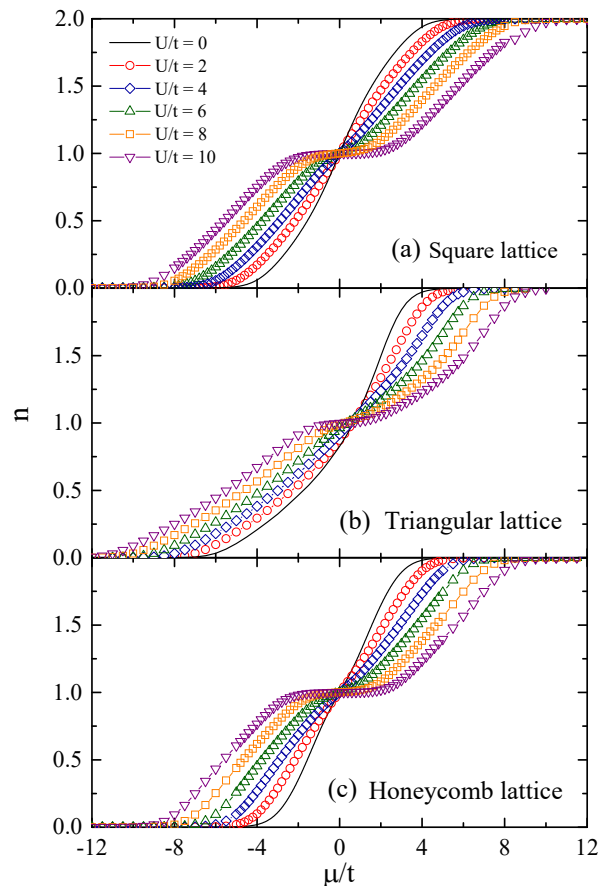

Figure 1. (Color online) Density n as a function of chemical potential μ for the (a) square, (b) triangular, and (c) honeycomb lattices, for fixed $T/t = 0.5$, and different interaction strengths U/t. Here, and in all subsequent figures, when not shown, error bars are smaller than symbol size. A Mott plateau is formed above a critical interaction strength which depends on lattice geometry. Note the width of this plateau is a measure of the charge gap or "Mottness".

As the Seebeck coefficient is obtained from the entropy, we now turn to discuss its behavior for these geometries. The entropy can be obtained from the electronic density, $n(\mu)$, by integrating it over the chemical potential μ,

$$s(\mu, T) = \int_{-\infty}^{\mu} d\mu \left. \frac{\partial n}{\partial T} \right|_{\mu}. \tag{7}$$

Here, we define a three point derivative for $dn/dT|_\mu$, using $\beta t = 1.8$, 2.0 and 2.2.

Figure 2 (a) displays $s(\mu, T)$ as a function of n for the square lattice. One may notice that, at $T/t = 0.5$, the results for $U/t = 2$ (red circles symbols) and $U/t = 4$ (blue diamond symbols) exhibit very similar behavior to the non-interacting one (solid black curve), once the temperature is high enough to destroy the correlation effects for such small interaction strengths. However as U/t increases, e.g. $U/t = 6$, 8, and 10 the entropy presents a local minimum at half-filling, being drastically
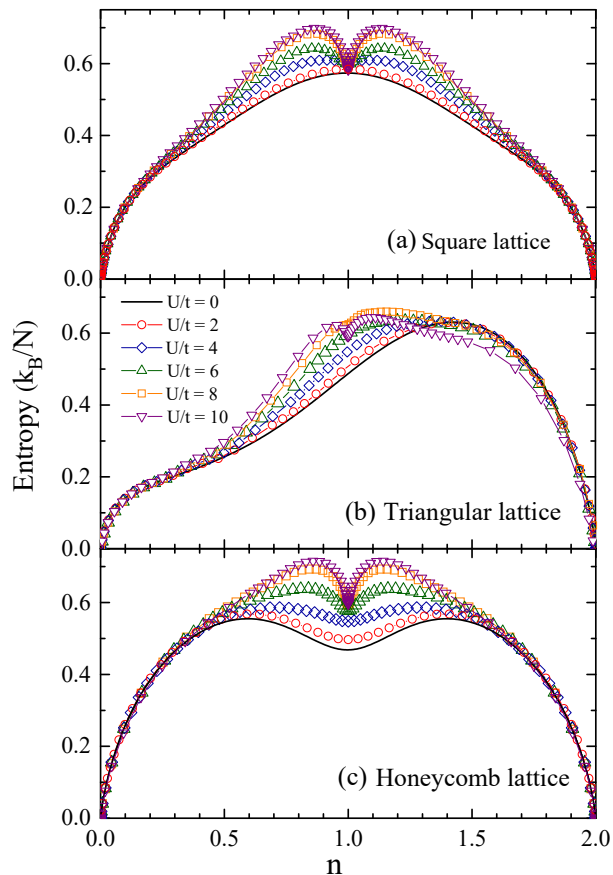
symmetry in the triangular lattice shown in Fig. 1 (c) is clearly also present in the entropy.

The entropy for the honeycomb lattice is more subtle. Similar to the square and triangular lattices, a local minimum appears at half-filling in presence of strong interaction; however, different from what is seen in the two previous cases, here $s(n,T)$ displays a suppression at half-filling even for the non-interacting case. This behavior is understood by recalling that the honeycomb lattice has a vanishing DOS at half-filling, with van Hove singularities below and above it. That is, the results of Fig. 2 confirm our expectations that the entropy provides hints about the DOS, irrespective of the interaction strengths. These odd features of the honeycomb lattice lead to strong changes for the Seebeck coefficient at $U = 0$, as we shall see in Section V, and may obscure some of the the electronic correlation effects.

IV. LOCAL DENSITY OF STATES AND CONDUCTIVITY

As discussed before, Fig. 1 signals the occurrence of a Mott insulating state due to the presence of a plateau in the density as a function of chemical potential, driven by correlations. The subtleties in the entropy, such as the appearance of a minimum for the noninteracting case at the half-filled honeycomb lattice [see Fig. 2(c)], in contrast to the square and triangular lattices [Figs. 2(a) and (b)], require an analysis of the suppression of spectral weight for different densities. In order to avoid numerical analytical continuations, we examine the LDOS only at the Fermi level ($\omega = 0$). Here we recall that, at the ground state, $N(\omega = 0) = \frac{dN}{d\omega} \propto \kappa(T = 0)$. Therefore, at finite temperatures, the thermodynamic DOS [14] is given by

$$N(\omega = 0, T) = \frac{dn}{d\mu} = n^2 \kappa(T) \qquad (8)$$

Fig. 3 shows $N(\omega = 0, T)$ for the (a) square, (b) triangular, and (c) honeycomb lattices. A common feature for all geometries is that the non-interacting case is an upper bound for the LDOS, with data close to the empty and completely filled systems showing a negligible dependence on the interaction strength. For the temperature shown, $T/t = 0.5$, we can see that for the square lattice and $U/t = 2$ the dip at half-filling has not developed yet. As correlations increase, the dip starts to form, leading to maxima at $n \approx 0.6$ and $n \approx 1.4$. In the case of the honeycomb lattice, the non-interacting ground state is known to be a semi-metal, with a vanishing LDOS at half-filling at $T/t \to 0$. Figure 3(c) shows a dip in the DOS at $T/t = 0.5$ already for $U/t = 0$, in line with entropy data. Similar to what is seen for the square lattice, maxima develop as correlations increase, but the positions are moved to $n = 0.5$ and $n = 1.5$. The triangular lattice LDOS shows a distinct behavior,

Figure 2. (Color online) Entropy s as a function of the electronic density n for the (a) square, (b) triangular, and (c) honeycomb lattices, for fixed $T/t = 0.5$, and different interaction strengths U/t. Note that the entropy is very different among the three lattices in the noninteracting limit. In presence of sufficiently large interactions, a local minimum appears at the half-filling for all three lattices; However, it becomes qualitatively similar for the square and honeycomb lattices, while it is different for the non-bipartite triangular lattice.

reduced as $T/t \to 0$, due to the Mott gap formation in the ground state [33, 35–38]. The increased entropy for the metallic state in the vicinity of half-filling in the presence of interactions has been observed for the cubic lattice and is relevant for cold fermionic atoms trapped in optical lattices, where the metallic region of the atomic cloud is used to absorb entropy and allow a central Mott region at a higher entropy per particle [39].

Unlike what is observed for the square lattice, the entropy behavior on the triangular geometry only exhibits such a local minimum at $U/t = 10$, the largest interaction strength considered, as presented in Fig. 2 (b). This suggests an absence of a Mott gap for weak and intermediate interaction strengths. In fact, at $U/t \gtrsim 8$, a small dip starts to form around $n = 1$, in line with the expectation for a metal-to-insulator transition occurring for $U/t \approx 7 - 8$ [40–42]. The lack of particle-hole
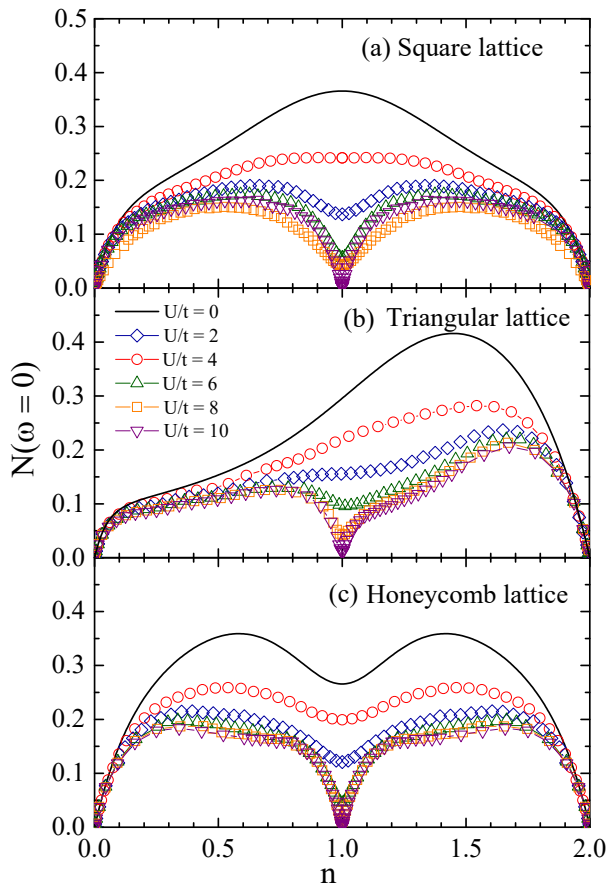
Figure 3. (Color online) Local density of states (LDOS) at the Fermi level at $T/t = 0.5$ as a function of density for the (a) square, (b) triangular, and (c) honeycomb lattices. Note the similarity of the doping dependence of LDOS to that of the entropy (Fig. 2) in the non-interacting limit. When correlations increase, LDOS develops a dip near half-filling, leading to maxima at intermediate densities which depend on the lattice geometry. The LDOS also becomes qualitatively similar to the square and honeycomb lattices in the strongly interacting limit, but is quite different from the triangular lattice which, in contrast, is not bipartite and has an asymmetric particle-hole many-body spectrum.

as can be seen in figure 3(b), with a broad peak for $U/t = 0$ located at $n \approx 1.6$. The effects of correlations are only relevant for $n \gtrsim 0.6$. For the larger values of U/t considered, a small broad peak is present at $n \simeq 0.75$ and a higher one at $n \simeq 1.6$, with a dip at half-filling signaling the Mott state for large U.

To further investigate the transport properties, we now turn to the longitudinal dc conductivity,

$$\sigma_{dc} = \frac{\beta^2}{\pi} \Lambda_{xx}(\mathbf{q} = \mathbf{0}, \tau = \beta/2), \qquad (9)$$

in which

$$\Lambda_{xx}(\mathbf{q}, \tau) = \langle j_x(\mathbf{q}, \tau) j_x(-\mathbf{q}, 0) \rangle \qquad (10)$$

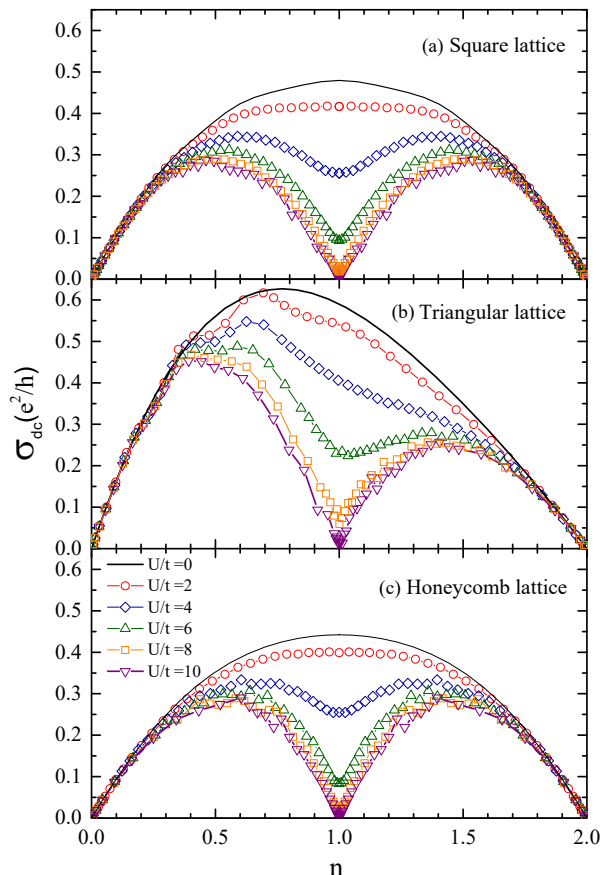is the current-current correlation function with $j_x(\mathbf{q}, \tau)$

Figure 4. (Color online) Longitudinal DC conductivity at $T/t = 0.5$ as a function of density for the (a) square, (b) triangular and (c) honeycomb lattices. The dip at half-filling signifies the opening of the Mott gap, and the presence (absence) of bipartiteness is reflected in the particle-hole symmetric (asymmetric) behavior of the conductivity. The locations of the peaks of $N(\omega = 0)$ are very different from that of σ_{DC} in the strongly interacting regime. Note that in the noninteracting case, $U/t = 0$, the dip in LDOS in Fig. 3 is not accompanied by a dip in σ_{dc} in the honeycomb lattice.

being the Fourier transform of the unequal-time current operator

$$j_x(\mathbf{i}, \tau) = \mathrm{e}^{\tau \mathcal{H}} \left[it \sum_\sigma \left(c^\dagger_{\mathbf{i+x}, \sigma} c_{\mathbf{i}, \sigma} - c^\dagger_{\mathbf{i}, \sigma} c_{\mathbf{i+x}, \sigma} \right) \right] \mathrm{e}^{-\tau \mathcal{H}}. \qquad (11)$$

Here we also avoid analytical continuation, see, e.g., Refs. 43–45.

Similar to what is seen for the LDOS, correlations reduce the conductivity, with the non-interacting conductivity as an upper limit for all the geometries studied as shown in Fig. 4. Once again, correlations are shown to be irrelevant to transport properties for densities near the completely empty or filled bands, while its effects increase as half-filling is approached, with $\sigma_{dc} \to 0$ as U/t increases. It is interesting to note that, for the honeycomb lattice, the dip in the non-interacting

DOS is not accompanied by a dip in the conductivity [shown in Figs. 3(c) and 4(c), respectively]. For large values of U/t, the maxima for the conductivity are not at the same densities as the ones for the LDOS; for the square lattice, the conductivity has maxima at $n = 0.5$ and $n = 1.5$. For the honeycomb lattice, the maxima are at $n = 0.6$ and 1.4 and for the triangular lattice, the maxima are at $n = 0.45$ and $n = 1.45$. For the triangular lattice, one can see that both the $U/t = 0$ peak and the higher intensity peak for the LDOS, which are above half-filling, move to densities below half-filling for the conductivity.

V. SEEBECK COEFFICIENT

We now turn to the Seebeck coefficient, which is obtained from the entropy by using the Kelvin formula [24, 46],

$$S_{\text{Kelvin}} = \frac{1}{e} \frac{\partial s}{\partial n} \bigg|_{T,V} . \qquad (12)$$

Within this approach, Fig. 5 displays the behavior of S_{Kelvin} in units of k_B/e^2 as a function of the electronic density for the (a) square, (b) triangular, and (c) honeycomb lattices.

At this point, it is worth recalling that the sign of the Seebeck coefficient is directly related to the type of carrier, being negative for holes and positive for electrons. As a consequence of particle-hole symmetry for the square and honeycomb lattices, one has $S_{\text{Kelvin}}(n) = -S_{\text{Kelvin}}(2 - n)$, leading to $S_{\text{Kelvin}}(n = 1) = 0$. For all geometries examined, the effect of correlations is strongly dependent on density, being negligible for $n \lesssim 0.3$ and $n \gtrsim 1.7$, as previously observed for entropy, DOS and conductivity.

As expected, the Seebeck coefficient for the non-interacting square lattice presents only one sign change, at half-filling, as shown in Fig. 5 (a). However, notice that in the presence of strong correlations ($U/t \gtrsim 6$) there is an anomalous behavior, characterized by a change of sign for densities away from half-filling, also displayed in Fig. 6 (a) for $n \approx 0.96$. In addition, there is a notable increase in the absolute value of the Seebeck coefficient, compared to the non-interacting case. For instance, at $n = 0.99$, $S_{\text{Kelvin}} \approx 2.37 \ k_B/e^2$, at $U/t = 10$, while for $U/t = 0$, $S_{\text{Kelvin}} \approx -0.01 \ k_B/e^2$. This steep increase can be explained by noting that the Seebeck coefficient, as defined in Eq. (3), is the ratio between the longitudinal thermoelectric and electrical conductivities. As we approach the Mott insulator at half-filling, electrons form local moments, and electrical transport is strongly reduced, as shown by both conductivity and LDOS in the previous section. The fast-decreasing electrical conductivity in the vicinity of half-filling must be accompanied by a non-vanishing thermoelectric current for the peaks to form. We can understand this as follows:
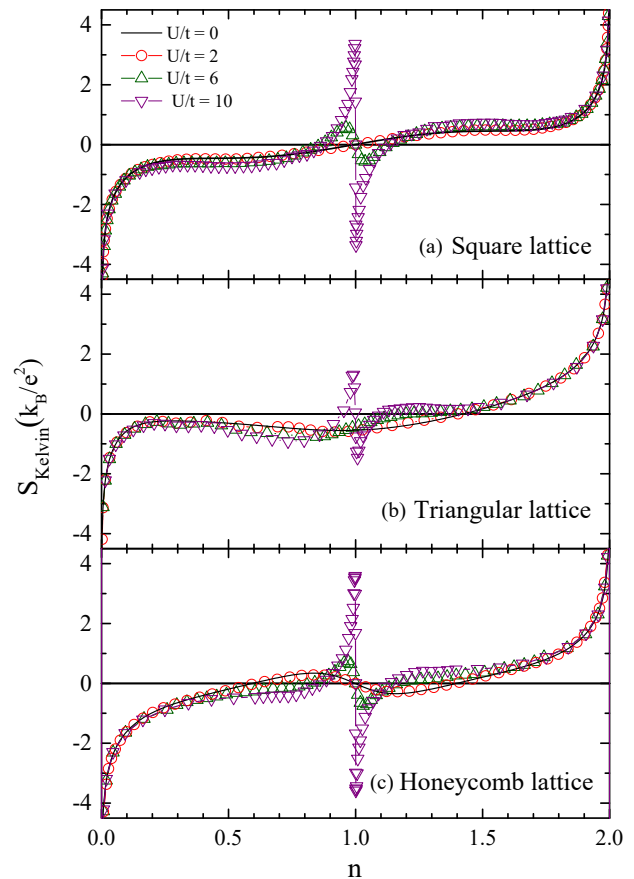

Figure 5. (Color online) Seebeck coefficient for different values of the interaction strength at $T/t = 0.5$ as a function of density for the (a) square, (b) triangular, and (c) honeycomb lattices. For clarity, we have reduced the set of U/t values compared to previous plots. In the non-interacting limit, the Seebeck coefficient changes sign at half-filling for bipartite lattices (square and honeycomb), but at a finite doping for triangular lattice. With strong interactions, there is an enhancement of the Seebeck coefficient near half-filling, as well as an anomalous sign changes away from half-filling, signaling a change in carrier type. Note that for the honeycomb lattice, there is a sign change in Seebeck coefficient away from half filling even at $U/t = 0$, due to presence of Van Hove singularities from the Bloch bands.

at half-filling and strong correlations, each site is singly occupied and local moments are completely formed, there is no electric or thermoelectric transport and the Seebeck coefficient is zero. As we move slightly away from half-filling, there is a background of local moments over which $p = 1 - n$ carriers lead to thermoelectric and electric currents. This reduced number of carriers is in line with the breaking of Luttinger count [47–49] that has been established for the Fermi Hubbard model and is in agreement with the change in carrier density in Hall experiments for YBCO [50].

Due to the absence of particle-hole symmetry in the triangular lattice, the sign change of S_{Kelvin} in the non-
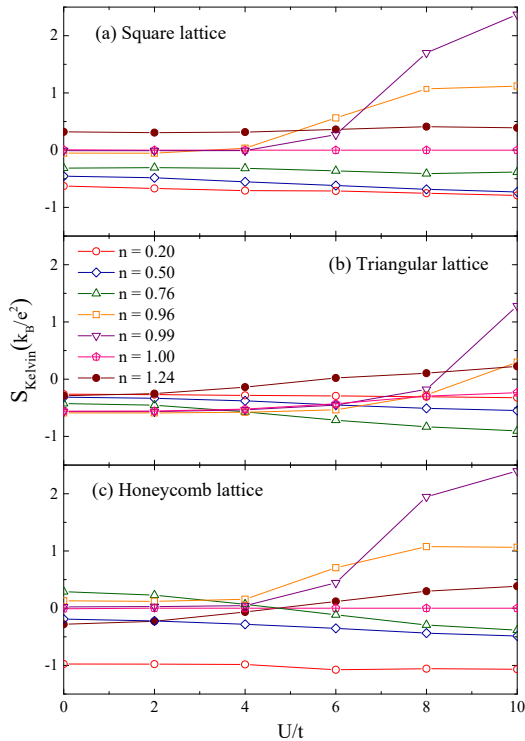
Figure 6. (Color online) Seebeck coefficient as a function of U/t, at a fixed $T/t = 0.5$ for different densities in (a) square, (b) triangular and (c) honeycomb lattices. For densities close to half-filling, the Seebeck coefficient changes sign and enhances as U/t is increased.

interacting limit occurs away from half-filling, at $n = 1.42$, as shown in Fig. 5 (b), as opposed to the square lattice, which has particle-hole symmetry, and exhibits the sign change symmetrically around half filling. There is a range of densities, around $0.5 \leq n \leq 0.9$ where correlations lead to a small increase in the modulus of the Seebeck coefficient. In contrast to the square lattice, the peak in the Seebeck coefficient for the triangular lattice at $n = 0.99$ is only present for very strong interactions. For $U/t = 8$, $S_{\text{Kelvin}} \approx -0.18 \ k_B/e^2$, while for $U/t = 0$, for this electronic density $S_{\text{Kelvin}} \approx -0.55 \ k_B/e^2$. Strong correlations, around $U/t = 10$, are needed to change the sign of the Seebeck coefficient at half-filling, as presented in Fig. 6 (b). Interestingly, above half-filling and below the sign-change point for $U/t = 0$, the correlations are detrimental to the thermopower up to $U/t = 8$, bringing the Seebeck coefficient closer to zero.

Fig. 5 (c) shows the Seebeck coefficient for the honeycomb lattice. For the non-interacting system, S_{Kelvin} changes sign at $n = 0.6$, 1.0, and 1.4, therefore the charge of the carriers is negative for $n < 0.6$ and $1.0 < n < 1.4$, while it is positive for $0.6 < n < 1.0$ and $n > 1.4$. Interestingly, these densities correspond to the peaks and dip positions for the conductivity, as seen in Fig. 4 (c). We recall that such changes in carriers come from the fact that the honeycomb lattice

has two bands for the noninteracting case, so one may expect changes from electron to hole properties of the transport coefficients depending on the filling of each band. However, correlations push the sign change to values closer to half-filling, going from $n = 0.6$ and 1.4 at $U/t = 0$ to $n = 0.85$ and 1.15 at $U/t = 8$. One thing to note is that although the behavior of the Seebeck coefficient is very different between the square and the honeycomb lattice in the noninteracting limit, adding interactions and transitioning to the Mott insulating state seems to wash these differences away. This can be understood by noting that in the noninteracting picture, the transport is determined by the Bloch bands which are different for square and honeycomb lattices. However, with strong interactions, Mott physics destroys the Bloch bands, opens up a Mott gap, and forms upper and lower Hubbard bands. While details of the single particle bands are erased, the information about the particle-hole symmetry imprinted in the many-body spectrum is still retained. Hence the behavior of the Seebeck coefficient is qualitatively similar between the square and honeycomb lattice but different from the triangular lattice.

Similar to the square lattice, there is a significant increase in the Seebeck coefficient for the honeycomb lattice close to half-filling at $U/t = 6$, 8 and 10, as shown for $n = 0.96$ and $n = 0.99$ in Fig. 6 (c). For $U/t = 10$, for example, we have that for $n = 0.99$, $S_{\text{Kelvin}} \approx 2.30 \ k_B/e^2$, while in the non-interacting case ($U/t = 0$) for this density value, $S_{\text{Kelvin}} \approx 0.03 k_B/e^2$, an enhancement of two orders of magnitude. At this point, it is worth recalling that the sign change of the Seebeck coefficient (for a given electronic density) is an unexpected feature for Fermi liquids, being usually related to a Fermi surface reconstruction in cuprates [15, 16]. Figure 6 describes such a non-Fermi liquid behavior for the geometries analyzed here, the energy scale for the sign change depends on the interaction strength and temperature of the system.

We also analyze the effects of temperature on the thermopower for the square lattice at $U/t = 10$. Figure 7 (a) displays S_{Kelvin} as a function of n for different T/t, while Fig. 7 (b) shows S_{Kelvin} as a function of T/t for different densities. The curves for different temperatures in [Fig. 7(a)] display narrow crossings in $\langle n \rangle = 0.53, 1.47$ leading to almost horizontal lines at these densities in Fig. 7(b). The presence of such narrow crossings suggests the existence of isosbestic points, which can reveal interesting physics [51]; for instance, the existence of sharp crossing points in the specific heat curves of strongly correlated systems is related to the fact that the high-temperature entropy is bounded and independent of the correlation strength [52], and has been observed for the square lattice Hubbard model [38]. Simulations for the $SU(N)$ Hubbard model show that narrow crossings on energy curves lead to unexpected scaling relations [53]. Here we see that for $n \lesssim 0.5$ and $n \gtrsim 1.5$ reducing the temperature is detrimental to the thermopower, as seen by a reduction of the modulus of the Seebeck coefficient
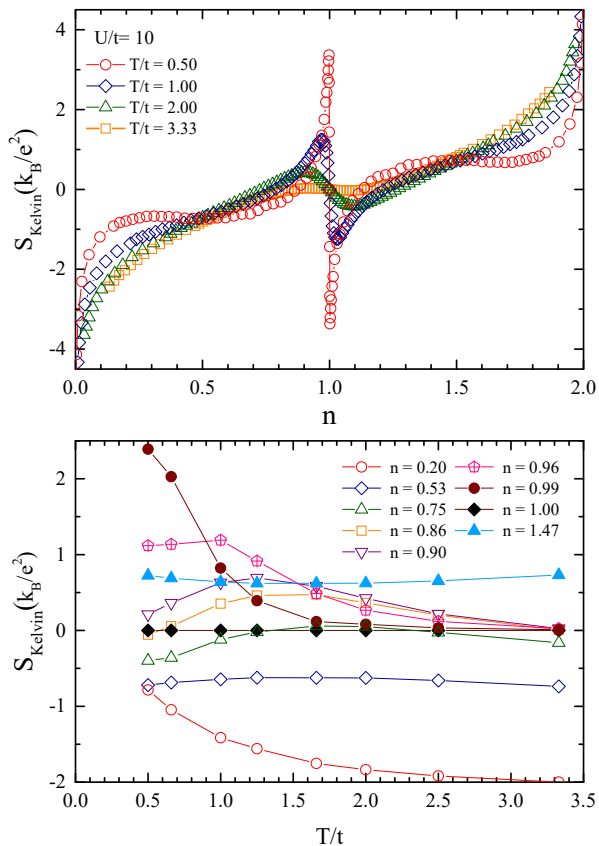
Figure 7. (Color online) Seebeck coefficient for the square lattice at $U/t = 10$ as (a) a function of density for the square lattice at different temperatures (b) a function of temperature for different densities. In panel (a), the Seebeck coefficient shows anomalous behavior at low temperatures and approaches the free particle limit as T/t is increased. In panel (b), at low densities ($n = 0.2$), the Seebeck coefficient has the expected sign and monotonically decreases with temperature. At a critical density $n \approx 0.5$ (also shown for $n \approx 1.5$ in the electron-doped side), the Seebeck coefficient is almost temperature independent. In the anomalous region ($0.75 \lesssim n \lesssim 1.0$), peaks in the Seebeck coefficient start to move towards the smallest temperature considered here, as one moves towards the half-filling limit, where it becomes 0 for all temperatures.

for $n = 0.2$. For densities in the range $0.5 \lesssim n \lesssim 0.9$ and $1.1 \lesssim n \lesssim 1.5$, the behavior of S_{Kelvin} with temperature is non-monotonic, and can change sign with T/t, as shown for $n = 0.75$ in figure 7(b). Finally, the anomalous behavior in the vicinity of half-filling has a marked dependence on temperature, increasing the modulus of the Seebeck coefficient as T/t is reduced. This fast increase of the thermopower with decreasing temperature close to half-filling has also been observed in the $t - J$ model[23], Hubbard model on an FCC lattice[24] and $t - t' - U$ Hubbard Model [14].
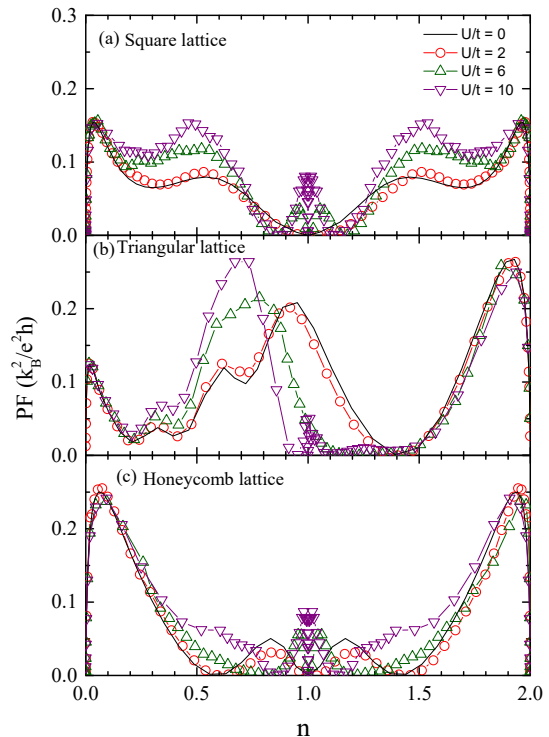

Figure 8. (Color online) Thermoelectric Power factor as a function of density for (a) square, (b) triangular, and (c) honeycomb lattices. In the free particle limit (almost empty and almost filled lattice), the Power factor exhibits a peak for all values of U/t. Interaction causes additional peaks to develop very close to the Mott insulating limit for large interaction strengths. Additional features for intermediate doping also appear that are strongly influenced by lattice geometry.

VI. THERMOELECTRIC POWER FACTOR

Proceeding, we now discuss the effects of correlations to the thermoelectric Power Factor (PF), defined as

$$PF = S^2 \sigma, \qquad (13)$$

where the dc conductivity (σ) and the Seebeck coefficient (S) were obtained in Sections IV and V, respectively. Simultaneously increasing both the modulus of the Seebeck coefficient and the conductivity maximizes the Power Factor. Strategies to determine the Seebeck coefficient that leads to an optimum thermoelectric Power Factor have been sought theoretically for systems that can be described by the Boltzmann transport equation [54] and experimentally for CZTS thin films [55] and La-doped $SrTiO_3$ [56] thin films.

Fig. 8 shows the thermoelectric Power Factor as a function of density for fixed $T/t = 0.5$, and for the three analyzed geometries. A common feature to all data is the presence of peaks close to the empty ($n \lesssim 0.1$) and completely filled lattices ($n \gtrsim 1.9$). Starting with

completely empty (filled) lattices, as density increases (decreases) the conductivity increases, and the Seebeck coefficient modulus decreases, leading to peaks that are independent of interaction strength. As the conductivity goes to zero for Mott insulators, $PF \rightarrow 0$ at half-filling for a geometry-dependent value of U/t. For the square lattice, the hump in PF for $U/t = 0$ around $n \approx 0.6$ (1.4) turns into a peak at $n \approx 0.5$ (1.5) with the increase of correlations, the dominant contribution coming from the conductivity.

The effect of correlations for the intermediate densities peak of the honeycomb lattice is more subtle, as can be seen in figure 8(c). The peaks for the non-interacting system at $n = 0.85$ ($n = 1.15$) decrease in intensity with correlations for $U/t = 2$ and 4, and then a shoulder develops at lower (higher) densities for larger U/t. Close to half-filling once again correlations drive the Seebeck coefficient peak up which in turn leads to the PF peaks.

For the triangular lattice one can see that the non-interacting system has a peak at $n = 0.95$. Correlations move the peak to lower densities and increase its intensity, as clearly seen in figure 8(b), where the peak for $U/t = 10$ is at $n \simeq 0.7$. As for the other geometries, a peak develops in the vicinity of the Mott insulating state, here only seen for the larger values of U/t studied.

Comparing the overall effects of correlations in the different geometries analyzed, we see that there are clear correlation-induced peaks near half-filling in all cases. For the square and honeycomb lattices, the non-interacting thermoelectric power factor is zero at half-filling and is driven to $PF \approx 0.1\ k_B^2/e^2 h$. Around quarter and three-quarter fillings as well, correlations also play a relevant role in increasing the power factor for the square and honeycomb lattices. Correlations are very effective in increasing the Power Factor in a triangular lattice, where $PF \simeq 0.27\ k_B^2/e^2 h$, the largest value obtained, for $U/t = 10$ at $n \sim 0.7$. For this geometry, we observe that density can be used to tune the thermoelectric Power Factor.

VII.   FINITE-SIZE EFFECTS

In this section, we investigate finite-size effects. To this end, we perform simulations for a 16×16 square lattice (i.e., with 576 sites), fixing $U/t = 8$, while varying the electronic density. Figure 9 displays (a) the longitudinal dc conductivity and (b) the Seebeck coefficient, for this system size, comparing it with our previous results for a 10×10 square lattice. Figure 9 clearly shows that, for these quantities, finite-size effects may be disregarded within the range of results examined in previous sections. Indeed, short-ranged quantities must suffer much less from finite-size effects than long-ranged quantities. However, these minor dependencies do not affect the main results discussed in the previous sections.
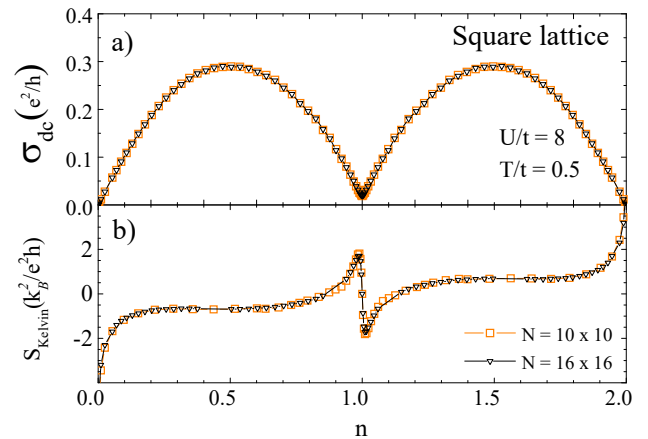

Figure 9. Comparison between results obtained for 10×10 (orange squares) and 16×16 (black triangles) lattices for (a) the longitudinal dc conductivity and (b) the Seebeck coefficient as a function of the electronic density at $U/t = 8$. When not shown, error bars are smaller than the symbol size.

VIII.   CONCLUSIONS

We have studied the thermoelectric properties of strongly interacting two dimensional systems with different geometries. Our results clearly show an anomaly in the Seebeck coefficient in the vicinity of half-filling, characterized by an enhanced response depending on both geometry and interaction strength. The anomaly is characterized by a change in the sign of the carriers which is accompanied by an interaction-induced increase. The anomaly is also intensified with the reduction of temperature.

The thermoelectric Power Factor displays a competition between the Seebeck coefficient and the conductivity. The anomaly in the Seebeck coefficient is reflected in the PF, with correlation-driven peaks immediately below and above half-filling at geometry-dependent values of U/t. The decreasing conductivity near half-filling is the limiting factor in the intensity of PF in this region of densities. Away from half-filling, at intermediate densities (around $n = 0.4 - 0.6$ and $n = 1.4 - 1.6$) the peaks in PF have a strong contribution from the conductivity with positions strongly dependent on geometry. For this range of densities, peak position and intensity can be tuned by correlations. Although the Seebeck coefficient is smaller for the triangular lattice, the Power Factor for this geometry shows the higher peak values and the stronger tunability with density and correlations, making it a strong candidate for enhanced thermoelectric properties.

APPENDIX

In this appendix, we discuss basic aspects of noninteracting and interacting cases related to the geometries examined in this work.

1. Dispersion and Density of States

The tight-binding approach for a single-band (s-wave) case leads to the following electronic dispersions,

$$E(k) = -2t(\cos k_x + \cos k_y), \tag{A.14}$$

$$E(k) = -2t\left[\cos\left(\frac{k_x + \sqrt{3}k_2}{2}\right)\cos\left(\frac{k_x - \sqrt{3}k_2}{2}\right) + \cos(k_x)\right], \tag{A.15}$$

$$E_\pm(k) = \pm t\sqrt{3 + 2\cos(k_x) + 2\cos(k_y) + 2\cos(k_x + k_y)}, \tag{A.16}$$

for the square, triangular, and honeycomb lattices, respectively. Here, we define t as the integral hopping for nearest neighbors, while assuming the lattice parameter as unity.

From the dispersion relation, one is able to obtain the Density of States ($N(\omega)$) for each geometry, as shown in Fig. 10. Notice that van Hove singularities (vHS) occur for all cases, as expected for noninteracting electrons in two-dimensional geometries. In particular, such a singularity is at half-filling for the square lattice but occurs at different fillings for the triangular and honeycomb ones. At finite temperatures, the vHS are smeared, with the occurrence of a cusp instead of divergence, as presented in Fig. 3. Furthermore, $N(\omega)$ also provides us hints of another important feature: the

existence of particle-hole symmetry (PHS). The PHS implies a symmetric distribution for electrons and holes, therefore leading to $\mu = 0$ for the half-filling and a symmetric DOS around it. Notice that these features are present in the square and honeycomb lattices, but are absent in the triangular one.

2. Critical points

For the repulsive Hubbard model, the interaction may lead to drastic changes in the DOS and other quantities' responses. In particular, some fillings may have instabilities, with the occurrence of phase transitions. From unbiased QMC methodologies, it is known that the Hubbard model at the half-filled square lattice exhibits antiferromagnetism for any $U/t > 0$ [57–59], while one has a finite critical point in the honeycomb lattice, for $U_c/t \approx 3.8$ [60–62]. By contrast, the ground state of the Hubbard model in the triangular lattice is less clear. In spite of this, there are pieces of evidence that a metal-insulator transition occurs around $U_c/t \approx 7$ [63–67].
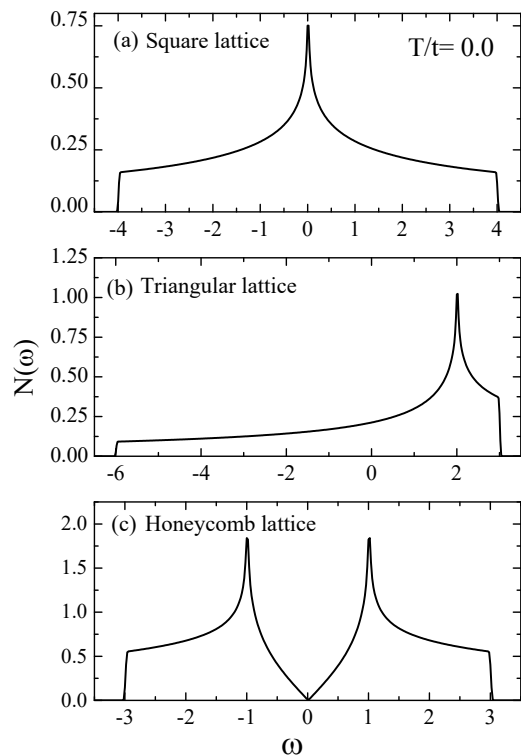
Figure 10. (Color online) Density of state as a function of ω for square (a), triangular (b), and honeycomb (c) lattices and $T/t = 0.0$

[1] S. Hébert, D. Berthebaud, R. Daou, Y. Bréard, D. Pelloquin, E. Guilmeau, F. Gascoin, O. Lebedev, and A. Maignan, Searching for new thermoelectric materials: some examples among oxides, sulfides and selenides, Journal of Physics: Condensed Matter **28**, 013001 (2015).

[2] G. Ding and J. Li, Band structure engineering of multiple band degeneracy for enhanced thermoelectric power factors in MTe and MSe (M = Pb, Sn, Ge), RSC Adv.

5, 91974 (2015).

[3] J. P. Heremans, V. Jovovic, E. S. Toberer, A. Saramat, K. Kurosaki, A. Charoenphakdee, S. Yamanaka, and G. J. Snyder, Enhancement of thermoelectric efficiency in PbTe by distortion of the electronic density of states, Science **321**, 554 (2008).

[4] L. D. Hicks and M. S. Dresselhaus, Effect of quantum-well structures on the thermoelectric figure of merit, Phys. Rev. B **47**, 12727 (1993).

[5] P. Wissgott, A. Toschi, H. Usui, K. Kuroki, and K. Held, Enhancement of the Na_xCoO_2 thermopower due to electronic correlations, Phys. Rev. B **82**, 201106 (2010).

[6] P. Wissgott, A. Toschi, G. Sangiovanni, and K. Held, Effects of electronic correlations and disorder on the thermopower of Na_xCoO_2, Phys. Rev. B **84**, 085129 (2011).

[7] J. M. Tomczak, Thermoelectricity in correlated narrow-gap semiconductors, Journal of Physics: Condensed Matter **30**, 183001 (2018).

[8] S. D. Obertelli, J. R. Cooper, and J. L. Tallon, Systematics in the thermoelectric power of high-t_c oxides, Phys. Rev. B **46**, 14928 (1992).

[9] J. L. Tallon, C. Bernhard, H. Shaked, R. L. Hitterman, and J. D. Jorgensen, Generic superconducting phase behavior in high-t_c cuprates: t_c variation with hole concentration in $yba_2cu_3o_{7-\delta}$, Phys. Rev. B **51**, 12911 (1995).

[10] T. Honma and P. H. Hor, Unified electronic phase diagram for hole-doped high-T_c cuprates, Phys. Rev. B **77**, 184520 (2008).

[11] T. M. Benseman, J. R. Cooper, C. L. Zentile, L. Lemberger, and G. Balakrishnan, Valency and spin states of substituent cations in $bi_{2.15}sr_{1.85}cacu_2O_{8+\delta}$, Phys. Rev. B **84**, 144503 (2011).

[12] A. Garg, B. S. Shastry, K. B. Dave, and P. Phillips, Thermopower and quantum criticality in a strongly interacting system: parallels with the cuprates, New Journal of Physics **13**, 083032 (2011).

[13] G. C. McIntosh and A. B. Kaiser, van hove scenario and thermopower behavior of the high-t_c cuprates, Phys. Rev. B **54**, 12569 (1996).

[14] E. W. H. B. M. Wen O. Wang, Jixun K. Ding and T. P. Devereaux, Quantitative assessment of the universal thermopower in the Hubbard model, arXiv:2302.13169 (2023).

[15] O. Cyr-Choinière, S. Badoux, G. Grissonnanche, B. Michon, S. A. A. Afshar, S. Fortier, D. LeBoeuf, D. Graf, J. Day, D. A. Bonn, W. N. Hardy, R. Liang, N. Doiron-Leyraud, and L. Taillefer, Anisotropy of the seebeck coefficient in the cuprate superconductor $yba_2cu_3o_y$: Fermi-surface reconstruction by bidirectional charge order, Phys. Rev. X **7**, 031042 (2017).

[16] A. Gourgout, G. Grissonnanche, F. Laliberté, A. Ataei, L. Chen, S. Verret, J.-S. Zhou, J. Mravlje, A. Georges, N. Doiron-Leyraud, and L. Taillefer, Seebeck coefficient in a cuprate superconductor: Particle-hole asymmetry in the strange metal phase and fermi surface transformation in the pseudogap phase, Phys. Rev. X **12**, 011037 (2022).

[17] L. Onsager, Reciprocal relations in irreversible processes. I., Physical Review **37**, 405 (1931).

[18] M. Jonson and G. Mahan, Mott's formula for the thermopower and the Wiedemann-Franz law, Physical Review B **21**, 4223 (1980).

[19] R. Heikes, R. Ure, and S. Angello, Thermoelectricity: Science and Engineering (Interscience Publishers, 1961).

[20] B. S. Shastry, Sum rule for thermal conductivity and dynamical thermal transport coefficients in condensed matter, Physical Review B **73**, 085117 (2006).

[21] B. S. Shastry, Electrothermal transport coefficients at finite frequencies, Reports on progress in physics **72**, 016501 (2008).

[22] L. Zdroj, Theory of dynamical thermal transport coefficients in correlated condensed matter, Lecture notes given at the 43rd Karpacz Winter School of Theoretical Physics on Condensed Matter Physics in the Prime of XXI Century:Phenomena, Materials, Ideas, Methods (2007).

[23] M. R. Peterson and B. S. Shastry, Kelvin formula for thermopower, Phys. Rev. B **82**, 195105 (2010).

[24] L.-F. Arsenault, B. S. Shastry, P. Sémon, and A.-M. S. Tremblay, Entropy, frustration, and large thermopower of doped mott insulators on the fcc lattice, Phys. Rev. B **87**, 035126 (2013).

[25] R. Blankenbecler, D. J. Scalapino, and R. L. Sugar, Monte Carlo calculations of coupled boson-fermion systems. I, Phys. Rev. D **24**, 2278 (1981).

[26] J. E. Hirsch, Discrete Hubbard-Stratonovich transformation for fermion lattice models, Phys. Rev. B **28**, 4059 (1983).

[27] J. E. Hirsch, Two-dimensional Hubbard model: Numerical simulation study, Phys. Rev. B **31**, 4403 (1985).

[28] S. R. White, D. J. Scalapino, R. L. Sugar, N. E. Bickers, and R. T. Scalettar, Attractive and repulsive pairing interaction vertices for the two-dimensional Hubbard model, Phys. Rev. B **39**, 839 (1989).

[29] J. Gubernatis, N. Kawashima, and P. Werner, Quantum Monte Carlo Methods: Algorithms for Lattice Models (Cambridge University Press, Cambridge, England, 2016).

[30] F. Becca and S. Sorella, Quantum Monte Carlo approaches for correlated systems (Cambridge University Press, Cambridge, England, 2017).

[31] R. R. dos Santos, Introduction to quantum Monte Carlo simulations for fermionic systems, Brazilian Journal of Physics **33**, 36 (2003).

[32] A. J. Kim, F. Simkovic, and E. Kozik, Spin and charge correlations across the metal-to-insulator crossover in the half-filled 2d Hubbard model, Phys. Rev. Lett. **124**, 117602 (2020).

[33] F. Simkovic, J. P. F. LeBlanc, A. J. Kim, Y. Deng, N. V. Prokof'ev, B. V. Svistunov, and E. Kozik, Extended crossover from a fermi liquid to a quasiantiferromagnet in the half-filled 2d Hubbard model, Phys. Rev. Lett. **124**, 017003 (2020).

[34] C. Lenihan, A. J. Kim, F. Šimkovic IV., and E. Kozik, Entropy in the Non-Fermi-Liquid regime of the doped 2D Hubbard model, Phys. Rev. Lett. **126**, 105701 (2021).

[35] J. Bonča and P. Prelovšek, Thermodynamics of the planar Hubbard model, Phys. Rev. B **67**, 085103 (2003).

[36] E. Khatami and M. Rigol, Thermodynamics of strongly interacting fermions in two-dimensional optical lattices, Phys. Rev. A **84**, 053611 (2011).

[37] K. Mikelsons, E. Khatami, D. Galanakis, A. Macridin, J. Moreno, and M. Jarrell, Thermodynamics of the

quantum critical point at finite doping in the two-dimensional Hubbard model studied via the dynamical cluster approximation, Phys. Rev. B **80**, 140505 (2009).

[38] T. Paiva, R. T. Scalettar, C. Huscroft, and A. K. McMahan, Signatures of spin and charge energy scales in the local moment and specific heat of the half-filled two-dimensional Hubbard model, Phys. Rev. B **63**, 125116 (2001).

[39] T. Paiva, Y. L. Loh, M. Randeria, R. T. Scalettar, and N. Trivedi, Fermions in 3d optical lattices: Cooling protocol to obtain antiferromagnetism, Phys. Rev. Lett. **107**, 086401 (2011).

[40] T. Yoshioka, A. Koga, and N. Kawakami, Quantum phase transitions in the Hubbard model on a triangular lattice, Phys. Rev. Lett. **103**, 036401 (2009).

[41] T. Shirakawa, T. Tohyama, J. Kokalj, S. Sota, and S. Yunoki, Ground-state phase diagram of the triangular lattice Hubbard model by the density-matrix renormalization group method, Phys. Rev. B **96**, 205130 (2017).

[42] D. Garwood, J. Mongkolkiattichai, L. Liu, J. Yang, and P. Schauss, Site-resolved observables in the doped spin-imbalanced triangular Hubbard model, Phys. Rev. A **106**, 013310 (2022).

[43] N. Trivedi, R. T. Scalettar, and M. Randeria, Superconductor-insulator transition in a disordered electronic system, Phys. Rev. B **54**, R3756 (1996).

[44] P. J. H. Denteneer, R. T. Scalettar, and N. Trivedi, Conducting phase in the two-dimensional disordered Hubbard model, Phys. Rev. Lett. **83**, 4610 (1999).

[45] R. Mondaini, K. Bouadim, T. Paiva, and R. R. dos Santos, Finite-size effects in transport data from quantum Monte Carlo simulations, Phys. Rev. B **85**, 125127 (2012).

[46] M. R. Peterson and B. S. Shastry, Kelvin formula for thermopower, Phys. Rev. B **82**, 195105 (2010).

[47] I. Osborne, T. Paiva, and N. Trivedi, Broken luttinger theorem in the two-dimensional Fermi-Hubbard model, Phys. Rev. B **104**, 235122 (2021).

[48] C. Gröber, R. Eder, and W. Hanke, Anomalous low-doping phase of the Hubbard model, Phys. Rev. B **62**, 4336 (2000).

[49] S. Sakai, Y. Motome, and M. Imada, Evolution of electronic structure of doped mott insulators: Reconstruction of poles and zeros of green's function, Phys. Rev. Lett. **102**, 056404 (2009).

[50] S. Badoux, W. Tabis, F. Laliberté, G. Grissonnanche, B. Vignolle, D. Vignolles, J. Béard, D. Bonn, W. Hardy, R. Liang, et al., Change of carrier density at the pseudogap critical point of a cuprate superconductor, Nature **531**, 210 (2016).

[51] M. Greger, M. Kollar, and D. Vollhardt, Isosbestic points: How a narrow crossing region of curves determines their leading parameter dependence, Phys. Rev. B **87**, 195140 (2013).

[52] D. Vollhardt, Characteristic crossing points in specific heat curves of correlated systems, Phys. Rev. Lett. **78**, 1307 (1997).

[53] E. Ibarra-García-Padilla, S. Dasgupta, H.-T. Wei, S. Taie, Y. Takahashi, R. T. Scalettar, and K. R. A.

Hazzard, Universal thermodynamics of an SU(n) fermi-hubbard model, Phys. Rev. A **104**, 043316 (2021).

[54] P. Pichanusakorn and P. R. Bandaru, The optimal seebeck coefficient for obtaining the maximum power factor in thermoelectrics, Appl. Phys. Lett. **94**, 223108 (2009).

[55] A. Ashfaq, J. Jacon, A. Ali, K. Mehboob, K. Mahmood, U. Rehman, W. Ahmad, S. Ikram, N. Amin, S. Tahir, M. I. Arshad, M. Ajaz un Nabi, and S. Hussain, Designing of seebeck coefficient and electrical conductivity in CZTS thin films for giant power factor, Ceramics International **46**, 9646 (2020).

[56] B. Jalana and S. Stemmerb, Large Seebeck coefficients and thermoelectric power factor of La-doped $SrTiO_3$ thin films, Appl. Phys. Lett. **97**, 042106 (2010).

[57] C. N. Varney, C.-R. Lee, Z. J. Bai, S. Chiesa, M. Jarrell, and R. T. Scalettar, Quantum monte carlo study of the two-dimensional fermion hubbard model, Phys. Rev. B **80**, 075116 (2009).

[58] M. Qin, H. Shi, and S. Zhang, Coupling quantum Monte Carlo and independent-particle calculations: Self-consistent constraint for the sign problem based on the density or the density matrix, Phys. Rev. B **94**, 235119 (2016).

[59] K. Seki and S. Sorella, Benchmark study of an auxiliary-field quantum Monte Carlo technique for the Hubbard model with shifted-discrete Hubbard-Stratonovich transformations, Phys. Rev. B **99**, 144407 (2019).

[60] T. Paiva, R. T. Scalettar, W. Zheng, R. R. P. Singh, and J. Oitmaa, Ground-state and finite-temperature signatures of quantum phase transitions in the half-filled Hubbard model on a honeycomb lattice, Phys. Rev. B **72**, 085123 (2005).

[61] F. F. Assaad and I. F. Herbut, Pinning the order: The nature of quantum criticality in the Hubbard model on honeycomb lattice, Phys. Rev. X **3**, 031010 (2013).

[62] Y. Otsuka, S. Yunoki, and S. Sorella, Universal quantum criticality in the metal-insulator transition of two-dimensional interacting Dirac electrons, Phys. Rev. X **6**, 011029 (2016).

[63] M. Capone, L. Capriotti, F. Becca, and S. Caprara, Mott metal-insulator transition in the half-filled Hubbard model on the triangular lattice, Phys. Rev. B **63**, 085104 (2001).

[64] P. Sahebsara and D. Sénéchal, Hubbard model on the triangular lattice: Spiral order and spin liquid, Phys. Rev. Lett. **100**, 136402 (2008).

[65] T. Yoshioka, A. Koga, and N. Kawakami, Quantum phase transitions in the Hubbard model on a triangular lattice, Phys. Rev. Lett. **103**, 036401 (2009).

[66] A. Szasz, J. Motruk, M. P. Zaletel, and J. E. Moore, Chiral spin liquid phase of the triangular lattice Hubbard model: A density matrix renormalization group study, Phys. Rev. X **10**, 021042 (2020).

[67] L. F. Tocchio, A. Montorsi, and F. Becca, Magnetic and spin-liquid phases in the frustrated $t - t^{'}$ Hubbard model on the triangular lattice, Phys. Rev. B **102**, 115150 (2020).